137 (2022) 212842

Contents lists available at ScienceDirect

Biomaterials Advances

journal homepage: www.journals.elsevier.com/materials-science-and-engineering-c

A hybrid thermoresponsive plasmonic nanogel designed for NIR-mediated chemotherapy

Julian Bergueiro [a,b,*,1], Emanuel A. Glitscher [a,1], Marcelo Calderón [a,c,d,*]

[a] Freie Universität Berlin, Institute for Chemistry and Biochemistry, Takustrasse 3, 14195 Berlin, Germany
[b] Centro Singular de Investigación en Química Biolóxica e Materiais Moleculares (CIQUS), Departamento de Química Orgánica, Universidade de Santiago de Compostela, 15782 Santiago de Compostela, Spain
[c] POLYMAT, Applied Chemistry Department, Faculty of Chemistry, University of the Basque Country UPV/EHU, Paseo Manuel de Lardizabal 3, 20018 Donostia-San Sebastián, Spain
[d] IKERBASQUE, Basque Foundation for Science, 48009 Bilbao, Spain

ARTICLE INFO

Keywords:
Nanogels
Thermoresponsive
Gold nanoparticles
Photothermal agent
cancer therapy
Nanocarrier
Drug delivery

ABSTRACT

Temperature-trigger chemotherapy is one of the state-of-the-art anti-tumoral strategies in nanomedicine. However, this strategy is in close relationship with the effect of the temperature in the tumor tissue. With high temperatures, the ablation of the tumor tissue can hinder a correct chemotherapy approximation. On the other hand, with moderate temperatures a negative vascularization that promotes the tumor growing is produced and competes with the chemotherapeutic effects. We have constructed one nanogel system composed of a thermoresponsive polymer cross-linked by plasmonic gold nanoparticles (AuNPs) for temperature-trigger chemotherapy. Doxorubicin loaded in the porous interior of the nanogel is released when the thermoresponsive network of the nanogel collapses due to the heat generated by the AuNPs upon near infra-red light irradiation. The hybrid nanogel system has been tested in vitro and in vivo, where it was observed that the temperatures reached in the in vivo NIR irradiation have an undesired effect on the inhibition of the tumor growth while the drug loaded systems considerably reduced the tumor sizes. This study shows the importance of design in temperature triggered antitumoral systems, where lower temperatures usually reached in practical situations due to light attenuation produced by the tissue can be positively utilized for enhancing the antitumoral effect of loaded drugs in the system.

1. Introduction

Gold nanoparticles (AuNPs) are nowadays established as diagnostic and therapeutic agents in various fields of biomedical research [1–5]. Principally, their theranostic applications like optical imaging [6], photo acoustic tomography [7,8], immune therapy [9], and photodynamic/photothermal therapy [10–13] are based on their characteristic plasmon resonance in visible and near infra-red (NIR) regions. Absorbance in the NIR biological window, excellent light-to-heat conversion capabilities, and absence of photobleaching make AuNPs superior light to heat transducers when compared to other commonly used photo-transducing agents (i.e., organic dyes or conducting polymers) [14]. The AuNP's absorbing maxima of the surface plasmon resonance depends on size and shape of the particles and thus their photothermal (PT) properties can be tuned by constructing different nano-morphologies [15–17].

Therefore, for targeting biomedical applications, it is of great convenience to tune the AuNPs absorption into the NIR regime. Mainly due to low absorption of the tissues at these wavelength and the high penetration depths of NIR light into them [10]. The most common strategy to tune the absorption of AuNPs into the NIR is to increase the particle's size and/or anisotropy. Such morphological modifications can be easily performed with a variety of established protocols [18–20]. Anisotropic AuNPs are efficient in converting NIR light into heat that results in a local hyperthermia when applied in a therapeutic scenario [21,22]. Synergistically, the strong PT conversion can be utilized for

* Correspondence to: J. Bergueiro, Centro Singular de Investigación en Química Biolóxica e Materiais Moleculares (CIQUS), Departamento de Química Orgánica, Universidade de Santiago de Compostela, 15782 Santiago de Compostela, Spain and M. Calderón, POLYMAT, Applied Chemistry Department, Faculty of Chemistry, University of the Basque Country UPV/EHU, Paseo Manuel de Lardizabal 3, 20018 Donostia-San Sebastián, Spain.
E-mail addresses: julian.bergueiro.alvarez@usc.es (J. Bergueiro), marcelo.calderon@polymat.eu (M. Calderón).
[1] These authors contributed equally.

https://doi.org/10.1016/j.bioadv.2022.212842
Received 17 February 2022; Received in revised form 11 April 2022; Accepted 1 May 2022
Available online 6 May 2022

triggering the transition of heat-sensitive materials like thermoresponsive polymers, which collapse above their lower critical solution temperature (LCST) [23]. Most likely found in literature, NIR-absorbing AuNPs are combined with LCST-polymers in a core-shell-like arrangement [24–26], allowing the AuNP-polymer particles to function as nanocarriers for targeted delivery and release of therapeutic agents under NIR irradiation [27–29]. Other strategies comprise the incorporation of large anisotropic AuNPs into a crosslinked polymeric network so called nanogel (NG). Conveniently, NGs are highly efficient in physically entrapping anticancer drugs in their polymeric shell and releasing them upon temperature triggered transition of the responsive polymer. These three-dimensionally cross-linked particles are known for their biocompatibility, tuneable size, volume-phase transition, and modulable pore size for the encapsulation of biomolecules [30–35]. Moreover, mild local hyperthermia is known to enhance the efficacy of chemotherapy [36], thus integration of NIR-absorbing AuNPs in polymeric nanocarriers have several synergistic benefits.

Unfortunately, when combining these promising systems with large sized AuNPs, they often suffer from drawbacks like poor biodistribution and insufficient excretion – due to the large size of the AuNPs itself – as well as low drug loading capacities and/or unreliable release mechanics [37,38]. Reported strategy for overcoming the mentioned size related issues is the incorporation of small AuNPs into thermoresponsive polymeric NGs [39]. Inconveniently, the usage of small size AuNPs limits their shape to pure spherical particles losing the anisotropy factor and consequently the efficient NIR absorption. Therefore, the combination of suitably sized and shaped NIR-absorbing AuNPs with polymeric NGs remains a challenge [40].

Here, we present a new strategy for the preparation of gold NGs (GAuNGs) composed of thermoresponsive linear poly(glycidyl ether) (tPG) chains cross-linked by small AuNPs. A large number of small spherical AuNPs could be integrated into a thermally responsive polymeric NG network as cross-linkers and grown in situ into anisotropic structures under controlled conditions to shift the absorbance profile to NIR region. The tPG is a LSCT polymer that follows a Flory-Huggins type I behaviour in water. It was chosen because of its biocompatibility, easy chemical adaptability, and tuneable thermoresponsive properties upon variation of the hydrophobic-hydrophilic balance with the monomer side chains on a random copolymerization [41–43]. We furthermore investigated the anisotropic GNGs (GAuNGs) for their PT conversion under NIR irradiation. Encapsulation and release were studied with doxorubicin (Dox) as model anticancer drug. Lastly, we proved the applicability of our system as anticancer platform by a series of in vitro and in vivo studies.

2. Results and discussion

NGs are promising materials for drug delivery-based applications and can be composed exclusively of organic materials [33,44,45], or by combining organic and inorganic segments [46,47]. In both cases, a suitable cross-linking unit is necessary to assure the formation of uniformly sized particles with a homogenous network. Here, three-dimensionally cross-linked gold decorated nanogels (AuNGs) were formed using two building blocks: a) di-azidated thermoresponsive poly (glycidyl ether) (N_3-tPG-N_3) and b) small spherical AuNPs capped with ligands exposing bicyclononyne moieties (Au@BCN) as crosslinker (Fig. 1A). Click chemistry — strain-promoted azide-alkyne-cycloaddition (SPAAC) — was used to link the building blocks due to the advantages raise by this biocompatible copper-free approach [48,49]. Small AuNPs show comparable sizes to commonly used cross-linking units [30,50]. AuNGs were synthesized by combining SPAAC with thermo-nanoprecipitation (TNP), a method for the formation of monodisperse tPG-based nanogels recently developed by our group. NGs with tuneable sizes between 80 and 200 nm can be easily synthesized by TNP by varying the polymer to crosslinker ratio or by the solvent and non-solvent ratio selection [51]. Generally, 1:20 (non-solvent:solvent)

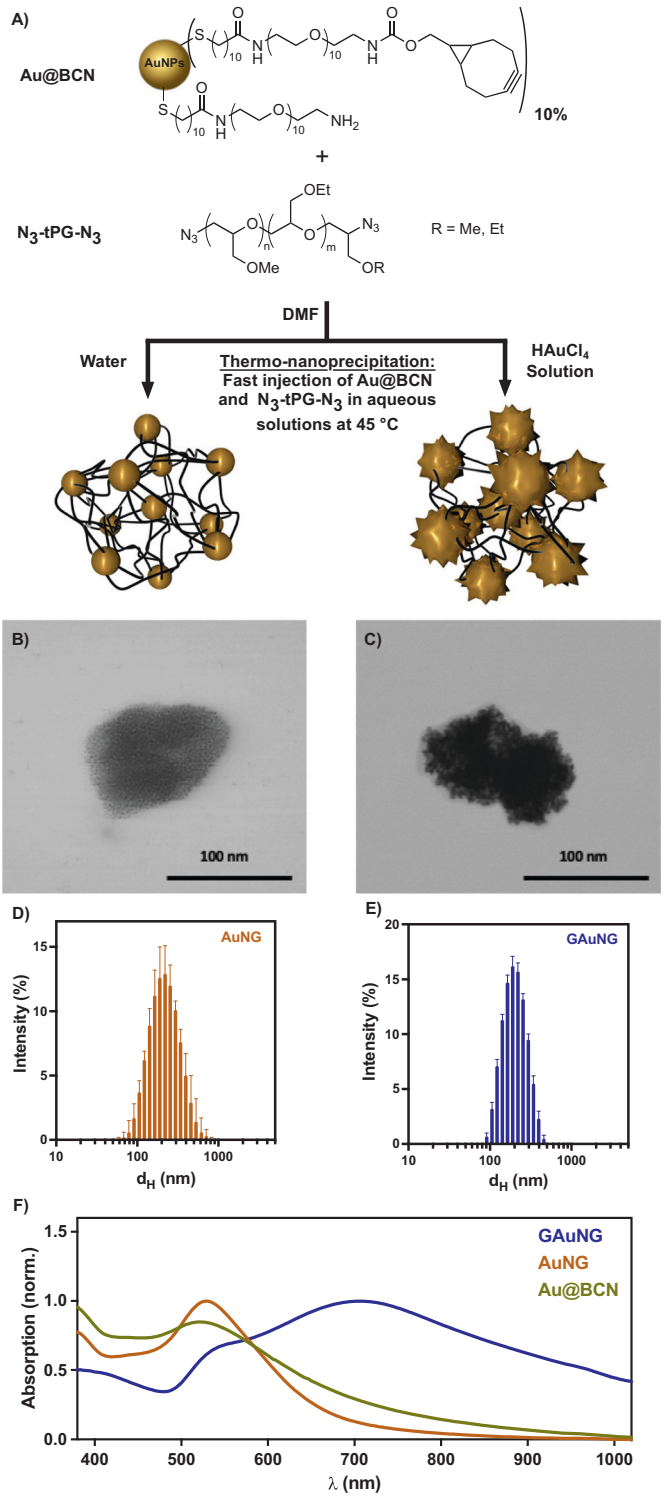

Fig. 1. A) Building blocks and routes to access AuNG and GAuNG through TNP. TEM images from B) AuNG and C) GAuNG. Hydrodynamic diameter distribution by DLS of D) AuNG and E) GAuNG. F) Overlayed UV–Vis spectra of Au@BCN, AuNG and GAuNG.

volume ratio affords particles in the range of 100–300 nm. Increasing the non-solvent volume increases the particle size and density whereas decreasing it has the oppose effect. Conveniently, for the targeted applications, particles in this size range are less likely to be removed from the bloodstream and therefore show prolonged circulation and accumulation in tumor tissue [52].

The precursor Au@BCN was formed in a modified Brust-Schiffrin approach by reduction of tetrachloroauric acid with sodium borohydride in water/dichloromethane with 11-mercaptoundecanoic ((aminoethoxy)-ethoxy)-ethyl amide (MUAA) as ligand [53]. The bicyclononyne (BCN) unit was introduced by amide coupling of N-succinimidyl protected bicyclo[6.1.0]non-4-yn-9-ylmethyl carbonate. Mean size of 3.8 ± 2.1 nm was confirmed by transmission electron microscopy (TEM) and statistical size analysis (Fig. S1). Functionalization degree of BCN (10%) was quantified by coupling with dansyl azide. The successful conjugation of alkyne moieties proposes Au@BCN as suitable cross-linking units for SPAAC.

As second building block, tPG with a molecular weight of 6 kDa was synthesized by anionic ring opening polymerization of the monomers glycidyl methyl ether (GME) and ethyl glycidyl ether (EGE). The feed ratio of monomers (1:1) used and the selected size guarantees the formation of tPG with a phase transition in physiological relevant temperature ranges [42]. Both ends of the polymer chains were converted into azides by mesylation and subsequent azidation. A polymer molecular weight of 6453 kDa was confirmed by gel permeation chromatography (GPC) and its thermo-sensitivity was validated by turbidimetry, showing a LCST of 35.9 °C in 1 mg mL^{-1} aqueous solution.

The synthesis of AuNGs followed a modified protocol for the formation of monodisperse particles by TNP [51]. Recently, we demonstrated the potential of using inorganic nanoparticles as cross-linkers for tPG NGs with magnetic iron oxide particles [54]. For the incorporation of AuNPs, Au@BCN and N_3-tPG-N_3 were solubilized and mixed in dimethylformamide (DMF) to induce cross-coupling by SPAAC and then precipitated in water at 45 °C (Fig. 1A). The ratio between solvent (DMF) and non-solvent (water at 45 °C) was carefully adjusted to allow the formation of stable dispersions. We applied a rational screening of the reactant ratios to yield particles with optimal sizes and dispersity. For that, the amount of polymer was kept constant while the amount of Au@BCN was varied in a range of 10 to 120 wt% corresponding to an azide/alkyne ratio of 1:0.1 and 1:1.7, respectively. In that range, optimal conditions were reached when using 60 wt% of Au@BCN (azide/alkyne ratio 1:0.8) in contrast to N_3-tPG-N_3. AuNGs synthesized with this ratio exhibit a hydrodynamic mean diameter (d_H) of 209.0 nm and a polydispersity index (PDI) of 0.222 confirmed by dynamic light scattering (DLS). Lowering the amount of Au@BCN results in formation of larger particles up to 400 nm due to the generation of less nucleation points that end up in bigger nanogels upon reactants consumption. On the other hand, when increasing the cross-linker content the number of nucleation points is increased as well and traduced in more irregular growing of the gels, thus leading to a slight increment in PDI.

For the use of the AuNGs as NIR transducers, we conveniently combined the described TNP protocol with a general procedure for the growth of anisotropic AuNPs [55]. With this novel approach we aim to merge structural growth of AuNPs into branched anisotropic nanoparticles with the formation of monodisperse NG particles to synthesize NIR absorption capable GAuNGs. Here, tPG and Au@BCN were again mixed in DMF but precipitated in a tetrachloroauric acid solution at 45 °C as non-solvent, immediately followed by the addition of ascorbic acid and silver nitrate. Ascorbic acid is used to reduce the gold ions in solution while silver nitrate acts as a shape determining agent for anisotropic growth of the seed Au@BCN particles (Fig. 1A). Instantaneous addition of all components is strongly required as growing at later stages results in non-homogeneous growth since the readily formed NGs remain in collapsed state at 45 °C and therefore shield the interior AuNPs from the growing components if not added together with the precursors. This indicates that the nucleation step in the TNP process in not altered by the gold growing conditions. After inducing the growth, we could detect a rapid change in colour from reddish to violet and blue indicating anisotropic expansion of AuNPs. For both AuNGs and GAuNGs, unreacted BCN-units were quenched with azidopropanol or, alternatively, with azidated poly(ethylene glycol) (PEG-N_3) for biological studies and the AuNGs were purified from remaining polymer chains, salts, and AuNPs by several dialysis and centrifugation steps. Coupling was confirmed via attenuated total reflectance Fourier transformed infra-red (ATR-FT-IR) spectroscopy by decrease of the typical peak for azides at 2100 cm^{-1} indicating triazole formation through SPAAC (Fig. S2). Moreover, control experiments with unfunctionalized gold particles or non-azidated tPG didn't afford nanogels in any case. Performing TNP under the same conditions except using MUAA functionalized AuNPs (Au@MUAA) without the necessary BCN-cross-linking units, we could not detect the formation of AuNGs neither in DLS nor TEM.

Both AuNGs and GAuNGs were compared regarding their physicochemical characterization (Table 1). The NGs develop similar d_H in water (205.3 and 189.2 nm, respectively) and show narrow size distributions (Fig. 1D,E) concluding that the additional growth did not affect the size range of the NG formation. Despite non-perfect star-like particles have been detected by TEM (Fig. 1C), the generated anisotropy generated successfully shifted the absorption maxima for GAuNGs to 707 nm as a result of the additionally applied growth when compared to AuNGs (530 nm) (Fig. 1F). Absorbance profiles also show a remarkable broadening for GAuNGs reaching from visible into NIR regime. This indicates anisotropic growth along several axes of the seed particles, as similar broadening can be observed for growing of highly asymmetric urchin- or star-like structures. This morphological change was observed by TEM and scanning electron microscopy (SEM) (Figs. 1C and S3). Both nanogels exhibit positive ζ-potentials resulting from amine-functionalization of the AuNPs (Fig. S4). Still GAuNGs show slightly lower values of +22.3 mV in contrast to +30.7 mV which we assign to shielding of the amine functions by interactions with the gold surface, as growing of the particles increases the individual surface volume of each particle and therefore decreases the total coverage density. The slight positive surface charge could help increase cellular uptake of the particles and is favourable for applications as drug delivery agent. Analysis by inductively coupled plasma optical emission spectrometry (ICP-OES) revealed the total amount of inorganic material inside the gels. While AuNGs show 20.1 wt% gold mass fraction, GAuNGs contribute with 22.5 wt% of gold plus silver to the mass fraction of inorganic material (Table 1). The low difference indicates that both nanogels contain high amounts of organic material, however the additional growth has a big influence in the plasmon resonance of the NGs.

TEM images showed the nature of the hybrid NGs (Fig. 1B,C). Both AuNGs and GAuNGs are visualized as spherical particles with a compact shape and a high number of AuNPs in the core surrounded by polymeric material. In contrast to AuNGs, the particles inside GAuNGs are slightly bigger and exhibit a distinct anisotropic shape resulting from the additional growth. In SEM, GAuNGs are also described by a more anisotropic-like shape. Our findings on the structural change of the AuNPs explain the red-shift and broadening of the absorption spectrum and therefore the ability of GAuNGs to act as phototransducers for NIR light. Sizes of the NGs in TEM/SEM collude with DLS measurements and with their uniform appearance. GAuNGs stored in aqueous solution do not exhibit changes in d_H for at least six months resulting from excellent colloidal stabilization through the ligation with tPG as already reported for other AuNP-polymer conjugates [56].

Temperature dependant phase transition was studied by turbidimetry experiments to determine the cloud point temperature (T_{cp}). NGs derived from tPG exhibit T_{cp} values between 32 and 45 °C dependant on the monomer feed ratio, the length of the tPG, the macromolecular cross-linker used, and the concentration of the NG itself. The synthesized AuNGs and GAuNGs show distinct phase transition in aqueous solutions of 1 mg mL^{-1} (Fig. 2A). For AuNGs, the T_{cp} was determined at 33.2 °C. GAuNGs exhibit similar T_{cp} at 32.3 °C for the same concentration. As the phase transition temperature of tPG material is highly dependent on the concentration in solution, we determined the T_{cp} of GAuNGs for lower concentrations, which are more relevant in context of biological evaluation. As previously reported for tPG-based NGs, the T_{cp} appear to rise with decreasing concentrations. At 0.5 mg mL^{-1} the transmittance curve

Table 1
Physico-chemical characterization for AuNG and GAuNG.

Nanogel	d_{HI} [nm]	PDI	ζ [mV]	λ_{max} [nm]	Au/Ag [wt%][a]	T_{max} [°C][b]	T_{cp} [°C][c]	DLC [%][d]
AuNG	205.3	0.222	+30.7	530	20.1	29.7	33.2	21.9
GAuNG	189.2	0.200	+22.3	707	22.5	94.3	32.3	27.0

[a] Gold and silver ions content determined by ICP-OES.
[b] T_{max} reached for a solution 0.2 mg mL^{-1} and irradiated with a 785 nm laser starting at room temperature.
[c] Measured in aqueous solutions of 1 mg mL^{-1}.
[d] Drug loading content for doxorubicin.

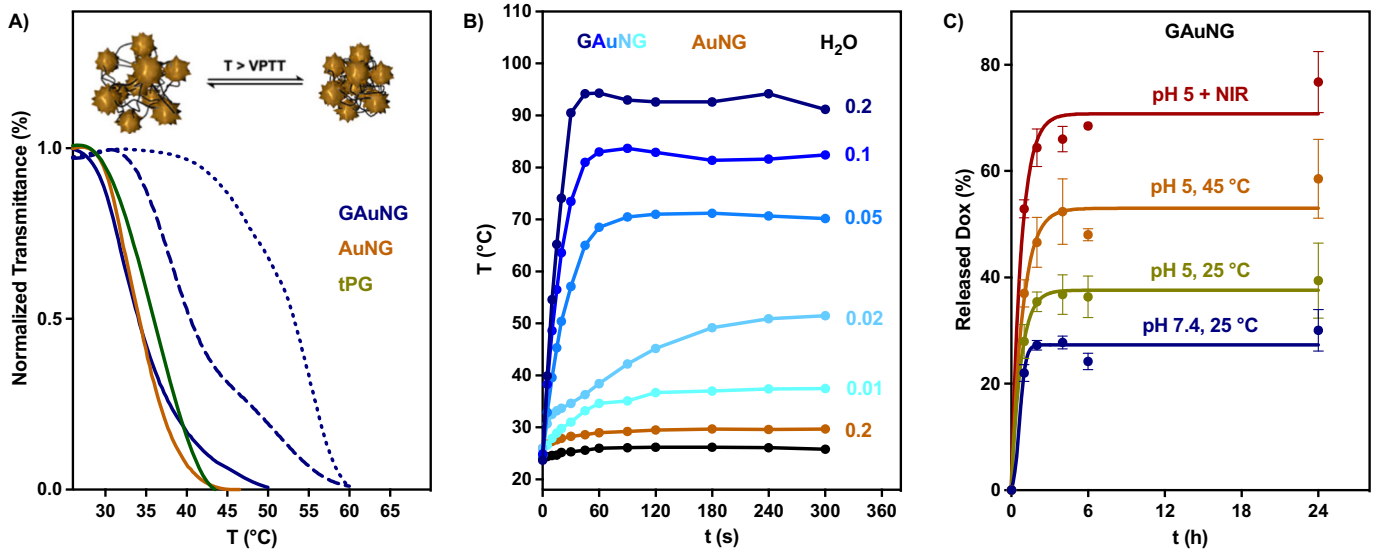

Fig. 2. A) Turbidimetry at 600 nm of 1 wt% aqueous solutions of tPG, AuNG, and GAuNG. GAuNG where measured in 0.5 wt% solution (dashed line) and 0.1 wt% solution (dotted line). B) Photothermal conversion of nanogels under irradiation with NIR laser (785 nm, 500 mW, 0.59 W cm^2). Concentration indicated in mg mL^{-1}. C) Cumulative release of Dox from GAuNG under different pH with or without NIR irradiation. The samples were kept at 25 °C if not otherwise indicated.

broadened and the cloud point was determined at 38.1 °C. Decreasing the concentration to 0.1 mg mL^{-1} led to even stronger broadening and two local minima of the first derivate at 46.8 and 54.9 °C. This can be contributed to less interactions between the NGs at lower concentrations. Measuring of the d_H against the temperature shows a reduction in size by half of the original d_H upon heating above the T_{cp} which is related to a decrease in volume when overpassing the volume phase transition temperature (VPTT) of the NGs (Fig. S5).

The photothermal conversion capability of GAuNGs was tested under irradiation with NIR light. For that, small volumes of the compound were irradiated from above with a 785 nm laser (500 mW, 0.59 W cm^{-2}) continuously for 5 min. The temperature was monitored with a FLIR thermal camera at different concentrations. At 0.2 mg mL^{-1}, the NIR-absorbing GAuNGs reached top temperatures of 94.3 °C in less than 60 s (Fig. 2B). Non-NIR-absorbing AuNGs do not exhibit significant increment in temperature at 0.2 mg mL^{-1}. Decreasing the concentration by one order of magnitude, GAuNGs still showed excellent heating profiles with maximum temperatures of 51.5 °C. Given that AuNPs exhibit local superheating of several hundred degrees under irradiation [21], we conclude that GAuNGs are undergoing VPTT under the given conditions even at low concentrations. The photothermal conversion efficiency (η) was determined to be 30.0% under observation of one heating and cooling cycle and is in good agreement with other AuNP-based systems used for biomedical approaches [57].

To evaluate the potential of GAuNGs as nanocarriers for small therapeutic molecules, GAuNGs were loaded with Dox for studying the uptake and release capacity of the hybrid particles. Encapsulation of Dox was achieved through hydrophobic interactions between the drug molecule and the AuNPs by incubating the NGs with Dox-solutions. AuNPs and hydrophobic drugs generally exhibit strong interactions and AuNP-based carrier systems develop high encapsulation rates [24]. Encapsulation for Dox solutions of 2 mg mL^{-1} showed a drug loading capacity (DLC) of 27.0%. Decreasing the initial concentration of Dox led to lower DLCs of 24.4% and 15.3% for 1 and 0.5 mg mL^{-1}, respectively (Fig. S6). Further increment of Dox concentration did not lead to a significant increase in DLC, as the saturation point of encapsulation is reached. The encapsulation efficiency (EE) changed from 30.1% for 0.5 mg mL^{-1} to values between 10 and 14% for higher concentrations. Optimal concentration for achieving high DLC and EE was determined to be 2 mg mL^{-1} for encapsulation of Dox in GAuNGs. Loading of Dox into GAuNGs shows superior DLCs compared with other AuNP-polymer systems, which usually exhibit values around 20–24% [24,58]. The higher DLC could result from the increased gold surface-to-volume ratio for GAuNGs compared to these systems and therefore more incorporation of Dox through hydrophobic interactions with the gold surface.

Release of Dox from the loaded GAuNGs was evaluated under different conditions. In acidic medium (pH 5), GAuNG-Dox showed enhanced release compared to neutral conditions thanks to the more favourable protonation of the Dox inside the nanogel (Fig. 2C). Altering the temperature above the VPTT of the NGs (42 °C) resulted in further increase and cumulative release of 58.6% after 24 h due to the increased hydrophobicity of the nanogel. Highest release of Dox was achieved when irradiating GAuNG-Dox at pH 5.0 with a NIR laser (785 nm, 500 mW, 0.59 W cm^{-2}) for 5 min before starting to monitor the release (76.8% cumulative release) due the fast change of the system to the hydrophobic state. We assume that the acidic pH results in Dox protonation and release from the hydrophobic domains of the GAuNGs, which can lead to an increased release in the slightly acidic environment of tumors and is additionally boosted by triggering the VPTT under NIR irradiation [52]. Release profiles show high similarity with comparable

Dox-loaded AuNP-nanocarriers, which also show high release rates up to 80% when exposed to acidic environment and/or under NIR irradiation [24,59].

After assessment of the physico-chemical properties, GAuNGs were studied regarding their biological behaviour in order to consider these systems as PT agents and nanocarriers in medical applications. To assure stability for biological characterization, the d_H of GAuNGs was measured in Roswell Park Memorial Institute (RPMI) cell culture medium and in human serum (HS) after incubation for 24 h (Fig. S7). In RPMI, the particles showed no difference in size (191.1 nm) whereas in HS, GAuNGs exhibit higher d_H (307.3 nm) due to strong association of serum proteins. Strong increase of d_H upon adsorption of serum proteins is also observed for other types of AuNPs and can be attributed to the positive surface charge of the NGs [60,61]. In both media, GAuNGs were

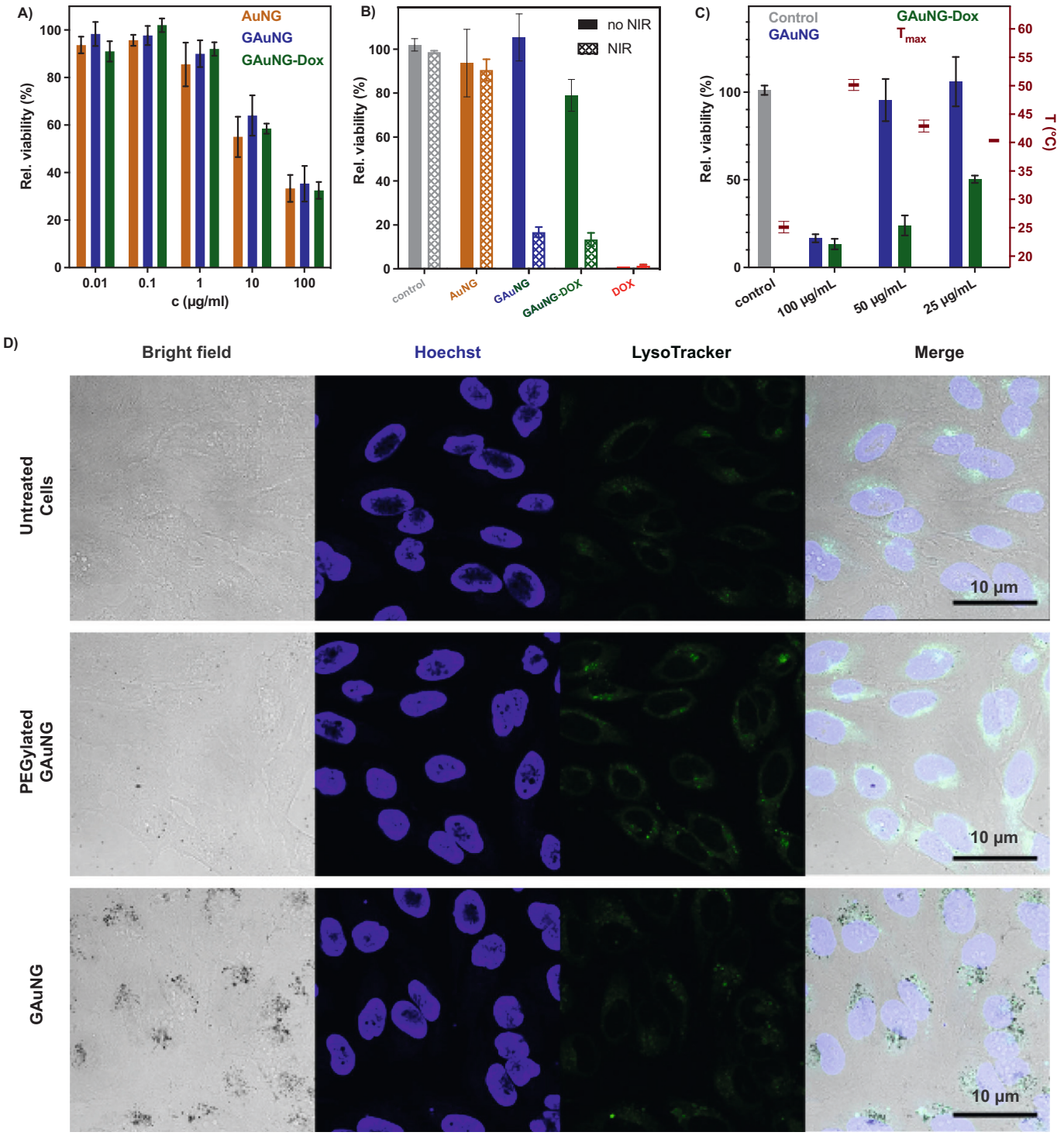

Fig. 3. A) MTT viability assay of AuNG, GAuNG, and GAuNG-DOX on HeLa cells. Cell viabilities determined by MTT assay for B) HeLa cells incubated with 100 μg mL^{-1} of AuNG, GAuNG, GAuNG-Dox, or 27 μg mL^{-1} free DOX before and after 3 min of irradiation with 785 nm laser and C) HeLa cells incubated with GAuNG and GAuNG-Dox at different concentrations of total nanogels after 3 min of irradiation. Dots indicate maximum temperatures reached during irradiation. D) Confocal microscopy images of HeLa cells incubated with cell culture medium containing no particles, PEGylated GAuNG, or GAuNG.

stable, and no signs of NG-to-NG aggregation could be detected.

For assessment of the impact on cell viability, the cytotoxicity of the gold containing NGs was evaluated on HeLa human cell line by MTT assay (Fig. 3A). Hela cells were incubated with the particles for 48 h. Incubation showed no reduction in viability up to 1 μg mL^{-1} and viabilities of 55–64% at concentrations of 10 μg mL^{-1}. The cytotoxicity profile of both AuNGs and GAuNGs showed high similarity concluding that the additional growing components do not decrease the cell viability on the tested cell line below the given values. The decrease in viability for the two highest tested concentrations can be attributed to the high density of the AuNPs resulting in faster sedimentation and interaction with cells in two-dimensional cell culture experiments [62]. Due to this, AuNP-based systems generally exhibit higher cytotoxicity in vitro than other nanomaterials and can cause oxidative stress and changes of cell morphology even at concentrations in the nM range [63]. Most gold nanomaterials cause decrease in cell viabilities in in vitro setups in the range of 1–100 μg mL^{-1}, which we also observed for our NGs [64]. Still, viabilities are sufficient for translation of the particles to therapeutic assays as the NIR-to-heat conversion is highly efficient even at low concentrations. Further loading of the GAuNGs with Dox also showed no significant effect on the cell viability indicating sufficient retention of the drug inside the NGs.

The potential of GAuNGs for photothermally induced chemotherapy of cells was hence studied by incubating human HeLa cells with AuNGs, GAuNGs, GAuNGs-Dox, or equivalent dose of free Dox. Cells incubated with the NGs showed dark colouring which remained after several washing steps and indicates that the particles were taken up by the cells or interacting with the cell membrane. The darkish coloured cell pellets, each with a volume of around 10 μL, were continuously irradiated with a 785 nm NIR laser for 3 min while the temperature was constantly monitored. Cell pellets incubated with GAuNG and GAuNG-Dox reached temperature plateaus between 48 and 51 °C after 45 s of irradiation. Cell pellets treated with AuNG, free Dox, or cell medium only did not show temperature increment upon NIR irradiation. Cells which were incubated with GAuNGs or GAuNGs-Dox and additionally irradiated showed a decrease in viability to a 20–40% compared to cells treated without irradiation (Fig. 3B). In contrast, cells which were incubated with non-NIR absorbing AuNGs showed no drop in cell viability after irradiation, as well as cells treated with medium only. Cells exposed to equivalent dose of free Dox showed viabilities of almost 0% with and without irradiation resulting from the high toxicity of Dox when not encapsulated in the NGs.

To further study the combinatory effect of local hyperthermia on chemotherapy, the concentrations of GAuNG and GAuNG-Dox for cell incubation were altered (Fig. 3C). At 100 μg mL^{-1} of NG concentration, both GAuNG and GAuNG-Dox reached mean temperatures of 50.1 °C and had a comparable effect on cell viability resulting from ablation by the strong heat generation. When decreasing the NG concentration to 50 μg mL^{-1}, the maximum temperature during irradiation dropped to 42.9 °C. As a result from this temperature decrement, treatment with unloaded GAuNGs reached cell viabilities around 100% for decreased concentrations. The viability for GAuNG-Dox-treated cells contrarily stayed below 30% and only slightly increased, when the concentration of the nanogels for cell incubation was again decreased to 25 μg mL^{-1}. Concluding, temperatures below 43 °C are not sufficient to result in cell death upon photothermal ablation but are adequate to induce a volume-phase transition of the thermoresponsive nanogels and release therapeutic amounts of the incorporated drug.

The interaction of GAuNGs with cells was studied by confocal microscopy to determine possible uptake of the particles by the cells (Fig. 3D). HeLa cells were incubated with the NGs for 16 h. The cells were thoroughly washed with PBS to remove remaining particles. In bright field, aggregates of the NGs can be clearly seen as black dots and co-localize with the LysoTracker, which indicates uptake of the NGs via endocytic pathway and intracellular transport through lysosomes, as observed for other gold-based nanomaterials [65,66]. As a negative control, GAuNGs decorated with PEG after the synthesis were used. In general, PEGylated AuNPs show significant drop in cellular uptake levels compared to non-PEGylated particles, which we could also observe in our set-up. This indicates that GAuNGs are fully or partially taken up by the used cell line which can be contributed to their surface charge, as positively charged AuNPs are favourably taken up by cells [67]. Further ICP-OES studies indicate a 67% of internalization efficiency.

As summary for the in vitro results, we aim to show the applicability of our system for heat-mediated chemotherapy in vivo. The minimum tolerated dose of AuNGs and GAuNGs was studied with healthy NMRI nude mice to evaluate sufficient doses and short-term toxicity. A two-step protocol was applied as followed: First, five doses with increasing amounts (10, 20, 40, 70, and 100 mg kg^{-1}) were injected intravenously through the tail vein and the mice were observed for a period of 15 days. As no signs of compound-related toxicity were observed, five injections of 100 mg kg^{-1} were performed for five consecutive days to reach a total accumulated dose of 500 mg kg^{-1}. One group of mice was sacrificed 1 day after the last treatment, a second group was kept for another 10 days without showing signs of toxicity or body weight loss (Fig. 4A). Organs were collected after treatment with the highest tolerable dose (liver, lungs, spleen, kidneys, and heart) for mice which were sacrificed 1 and 10 days after the last treatment, respectively, and their total weight was determined (Fig. S8). No signs of acute or chronic inflammation could be observed [68]. Collected histograms of all organs furthermore showed no specific findings on tissue alteration or inflammatory infiltrations for both AuNGs and GAuNGs (Fig. S9). Following the results from previous in vitro studies, AuNGs and GAuNGs show similar toxicity and tolerability patterns and GAuNGs are safe to use for further in vivo studies regarding their biodistribution and therapeutic efficacy.

Next, the biodistribution and tumor accumulation of GAuNGs was studied with tumor-bearing female NMRI nude mice. Evaluation of the biodistribution profile is crucial regarding the use of GAuNGs as drug delivery agents, as the optimal time point of highest accumulation in the targeted tissue needs to be determined for triggering the release of the drug and yielding maximum therapeutic efficiency. For detection of the administered material in organs and tumors, the metallic nature of the NGs was exploited to determine the amount of gold and silver ions by ICP-OES. The organs (liver, lung, spleen, kidney, heart, and tumor) were excised from A549 adenocarcinomic tumor bearing mice at several time points after injection of the particles through the tail vein. Highest concentrations of GAuNGs were detected in the liver, followed by smaller amounts of compound in spleen, lung, and tumor tissue (Fig. 4B). High accumulation in organs of the reticuloendothelial system is observed for many nanomaterials since particles in this size range (particularly pegylated ones) are targeted by macrophages through adsorption of opsonins [52]. Heart and kidneys showed no increased accumulation. In the tumor, concentrations of 0.02 mg mL^{-1} of gold plus silver ions were found after 6, 12, and 24 h (Fig. 4C). Considering the amount of inorganic material inside GAuNGs to be 22.5 wt% measured by ICP-OES, a total NG concentration of 0.09 mg mL^{-1} is reached. As previously shown, GAuNGs are able to reach temperatures sufficient for photothermal ablation and triggering of the VPTT under NIR irradiation at the given concentrations. 24 h timepoint after intravenous injection was considered to be the optimal time point for therapeutic NIR irradiation as all mice at this time point showed a similar accumulation pattern and sufficient concentrations. Furthermore, GAuNGs showed partial clearance from the tumors and organs after 48 h indicating that the most part of the particles are removed from the system. Dissections of the organs show black discolouration for liver and spleen as the particles show main accumulation in these organs (Fig. S10).

After proving biocompatibility and sufficient accumulation in tumor tissue, the therapeutic effect of GAuNG and GAuNG-Dox on the tumor volume with and without NIR irradiation was studied. For that, again A549 xenograft tumor bearing mice were chosen and doses of 100 mg kg^{-1} were injected intravenously through the tail vein. Tumors were

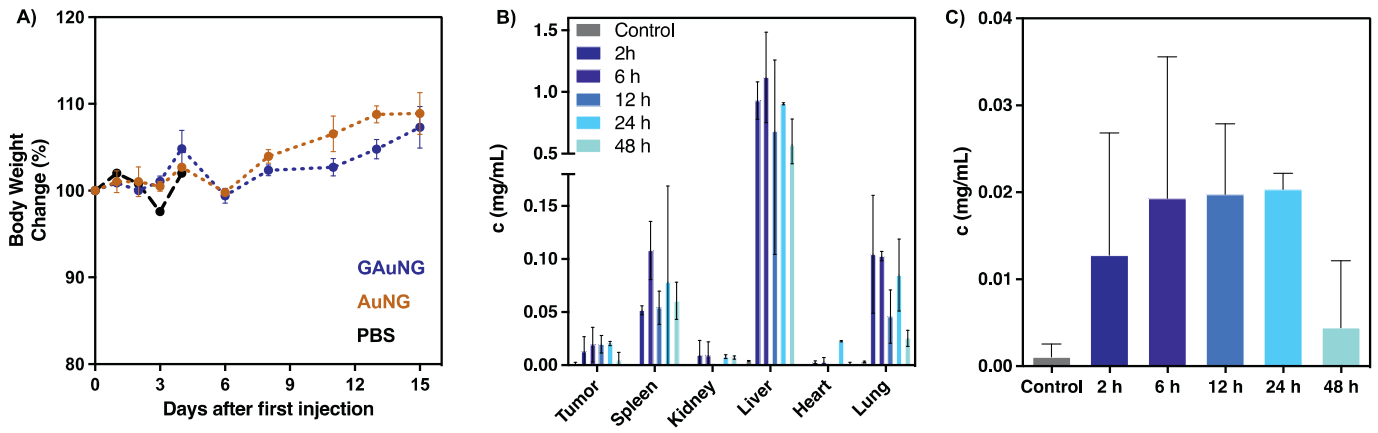

Fig. 4. A) Body weight change for mice treated with maximum tolerable dose of five times 100 mg kg^{-1}. B) Biodistribution of GAuNGs at different time points, measured by ICP-OES. C) Concentration of GAuNGs reached in tumor at different time points, measured by ICP-OES.

irradiated with NIR light after 24 h concluding from previous biodistribution study. As a general concept, the GAuNGs are converting the NIR light into heat triggering the phase transition of the polymeric material and promoting the release of incorporated Dox at the targeted site. GAuNGs without Dox-loading are administered to determine the effect of heat alone on the tumor growth. A noticeable inhibition in tumor growth for mice treated with GAuNG-Dox could be detected (Fig. 5A). Best therapeutic efficacy was achieved with GAuNG-Dox under NIR treatment, which resulted in relative tumor volume decrease by the factor 0.6 after completion of the treatment in contrast to control mice. For both groups treated with GAuNG-Dox, with and without irradiation, tumors showed reduced volume also compared to treatment with free Dox. Assumingly, Dox is already released from the NGs upon entering acidic tumor environment, as enhanced release was previously observed at pH 5.0. Surprisingly, tumors exhibited fastest growth with only GAuNGs plus NIR which can be related to the temperature increment which alone results in higher blood flow and perfusion to the tumor without sufficiently ablate the tumor cells [69]. Temperature-monitoring of the tumors during irradiation, however, was inconclusive, as the particles were potentially distributed throughout the whole tumor volume and irradiation only targeted a small area of the tumor. To achieve better monitoring over the temperature, we additionally applied doses of 30 μL (12 mg mL^{-1}) intratumorously followed by irradiation at the injection site. Thus, the local concentration of NGs was increased and the temperature raised to around 44–45 °C upon irradiation. The laser power was adjusted to maintain temperatures at this range for the purpose of preventing skin damage by excessive heat.

All intratumorously treated groups showed slight decreases in relative tumor volumes compared to intravenously injected samples, but overall tendency was not changed (Fig. S11). GAuNG-Dox was inhibiting tumor growth up to factor 0.5 with and without NIR whereas unloaded GAuNGs under NIR irradiation still exhibited biggest tumor volumes showing that the developed heat alone is not sufficient to reduce the tumor volume by thermal ablation. In fact, efficient tumor reduction through photothermal therapy requires temperatures of at least 47–48 °C [70], which we could not achieve in our set-up. Nevertheless, GAuNG-Dox was proven to inhibit tumor growth with and without NIR.

Furthermore, the particles were well tolerated reflected in a constant increment of body weight throughout the whole study (Fig. 5B). According to body weight change, only mice treated with free Dox exhibited decreasing body weights due to the toxic effects of the drug itself. After completion of treatment and dissection of the tumors, mean tumor weights show significant differences between mice treated with PBS and GAuNG-Dox with/without irradiation (Fig. 5C). Mice treated with free Dox also showed a reduction in tumor weight, but not as pronounced as for the loaded nanogels. In particular, tumors excised

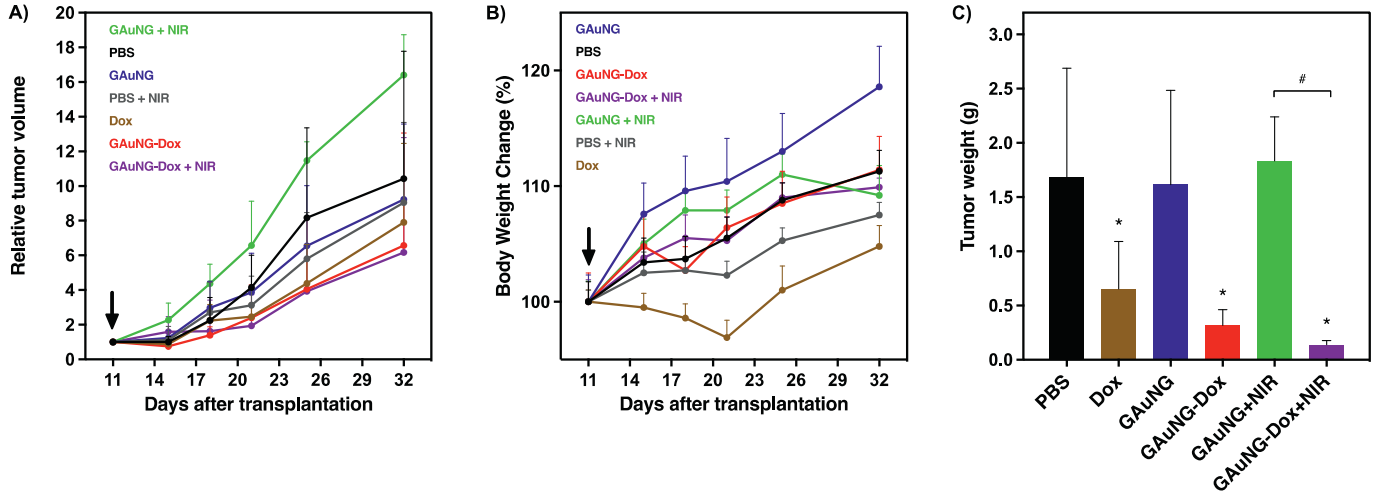

Fig. 5. A) Relative tumor volume at different time-points after intravenous (*i.v.*) application of nanogels and treatment with and without NIR irradiation. PBS and free Dox were always administered intravenously. B) Mean body weight change for intravenously administered nanogels. Arrows indicate the NG injection. NIR irradiation performed 24 h after injection. C) Weight of excised tumors after completion of treatment for intravenously administered nanogels. $*p < 0.1$, significant difference compared to PBS group; $\#p < 0.1$, significant difference between GAuNG and GAuNG-Dox with NIR irradiation.

from the GAuNG-Dox plus NIR treated group had around half the size than GAuNG-Dox without NIR treated groups, and around 20% the weight of the group treated with free Dox. Clearly, an effect of the directed delivery of the drug inside the nanocarrier is visualized here. Moreover, the effect could be even enhanced upon NIR irradiation and heating of the tumor microenvironment, whereas applying heat alone through unloaded NGs only resulted in a stronger growth. Concluding from this, NIR-mediated heat development caused by GAuNGs has to be accompanied by chemotherapeutic drug delivery to show a combinatorial effect on tumor growth inhibition. Images of the dissected tumors support these findings as tumors in the combinatorial group show lowest sizes (Fig. S12).

3. Conclusions

In this work, we presented for the first time the design of novel thermoresponsive gold-based NGs as efficient NIR-mediated nanocarriers. AuNGs were synthesized by cross-linking azidated thermoresponsive tPG with BCN-functionalized AuNPs. In a newly developed procedure, the AuNGs were simultaneously grown to GAuNGs during the synthesis resulting in an absorbance shift from visible to NIR region. Both AuNGs and GAuNGs show sizes around 200 nm and a phase transition above body temperature for concentrations below 0.5 mg mL^{-1}. Irradiation with NIR light resulted in strong light-to-heat conversion exclusively for GAuNGs. Furthermore, the GAuNGs were loaded with a high amount of Dox and the release was enhanced under NIR irradiation as the developed heat triggers the phase transition of the polymeric component and boosts release of the drug. The synergistic effect of developed heat on the targeted chemotherapeutic approach was hence proven in vitro. Cells incubated with GAuNG-Dox showed low viabilities exclusively under mild NIR irradiation by reaching temperatures above the VPTT followed by release of Dox from the NGs. In vivo studies with mice conclude, that GAuNGs are highly tolerable and lead to a tumor growth inhibition when loaded with Dox and additionally irradiated with NIR light. GAuNGs had high efficacy for photothermally induced chemotherapy and can therefore be considered as promising candidates for drug delivery applications.

4. Materials and methods

4.1. Materials

All chemicals were purchased from Sigma-Aldrich, Acros Organics, or Merck and used as received. Glycidyl methyl ether (GME) and ethyl glycidyl ether (EGE) were provided by TCI Europe, distilled, and stored over molecular sieves (5 Å) before usage. Doxorubicin hydrochloride was purchased from Yick-Vic Chemicals & Pharmaceuticals. 3-Azidopropanol was synthesized as described elsewhere [71]. Dry solvents were either purchased from Acros Organics or provided by a MBRAUN SPS 800 solvent purification system. Water used for the experiments was obtained from a Millipore water purification system (18.2 MΩ·cm).

4.2. Synthesis of N_3-tPG-N_3

The synthesis of tPG_{6kDa} was performed by anionic ring opening polymerization according to Carlotti et al. [72] Tetraoctylammonium bromide (TOAB) (2.1 mmol) was dried prior to the reaction under reduced pressure and dissolved in dry toluene (110 mL). After the addition of GME (55 mmol) and EGE (55 mmol), the solution was cooled down to 0 °C followed by the addition of *i*-Bu_3Al in hexanes (C = 1 M, 4.2 mmol). The reaction was proceeded for 16 h and then quenched with methanol (8 mL). The solvent was completely removed under reduced pressure and the crude product was dissolved in ice cold diethyl ether. The precipitated aluminum salt was removed by filtration and the ether was evaporated. This procedure was repeated until no further precipitation was observed. After dialysis against methanol (molecular weight cut-off, MWCO = 5000 Da), the product (0.83 mmol) was dried under vacuum and dissolved in dry THF (25 mL), followed by the addition of triethylamine (20 mmol). Methanesulfonyl chloride (10 mmol) was added dropwise at 0 °C. The reaction was carried out for 20 h at room temperature. The resulting yellow precipitate was removed by filtration and washed with THF. After evaporation of the solvent, the residues were purified by dialysis against methanol (MWCO = 5000 Da). The mesylated tPG_{6kDa} (0.6 mmol) was dried under vacuum and dissolved in dry DMF (10 mL). A solution of sodium azide (7.2 mmol) in dry DMF (10 mL) was added dropwise. The reaction stirred at 80 °C for 3 days and remaining salts were removed by filtration. After dialyzing against THF (MWCO = 5000 Da), the solvent was removed in vacuo to obtain a colourless oil (3.0 g, 30% over three steps). ^{1}H NMR (400 MHz, $CDCl_3$): δ (ppm) = 3.33–3.65 (m, polymer backbone), 3.31 (s, -OC$\underline{H}_3$), 1.14 (t, -OCH$_2$C$\underline{H}_3$) (Fig. S12). FT-IR: ν (cm^{-1}) = 2867, 2100, 1461, 1382, 1110, 917, 730. GPC: M_n = 6453 g/mol, M_w = 6897 g/mol, M_z = 7313 g/mol, PDI = 1.07.

4.3. Synthesis of MUAA

11-Mercaptoundecanoic acid (5 mmol), 4-dimethylaminopyridine (DMAP) (3 mmol), and hexafluorophosphate azabenzotriazole tetramethyl uronium (HATU) (12.5 mmol) were dried under reduced pressure and dissolved in dry DCM (60 mL). After stirring for 1 h, the solution was added dropwise to a solution of 2,2′-(ethylenedioxy)bis (ethylamine) (11.5 mmol) in dry DCM (120 mL) at 0 °C. After further stirring for 16 h at room temperature, the reaction was quenched with saturated $KHSO_4$-solution (150 mL) and extracted four times with DCM. The combined organic phase was dried with $NaSO_4$ and concentrated in vacuo. Column chromatography with DCM, methanol (8%), and TEA (1%) obtained a white solid (1.59 g, 91.3%). ^{1}H NMR (400 MHz, $CDCl_3$): δ (ppm) = 8.48 (s, 1H, N$\underline{H}$), 3.28 (q, 2H, S-C$\underline{H}_2$), 3.06–3.25 (m, 6H, CH_2-O-CH_2–), 2.29 (t, 2H, OC-C$\underline{H}_2$), 1.53–1.73 (m, 4H, -C$\underline{H}_2$), 1.38 (t, 1H, S$\underline{H}$), 1.15–1.35 (m, 12H, -C$\underline{H}_2$) (Fig. S13).

4.4. Synthesis of BCN-functionalized AuNPs

TOAB (0.4 mmol) was dissolved in DCM (20 mL). Tetrachloroauric acid trihydrate (0.1 mmol) in water (4 mL) was added and the two-phase mixture was stirred vigorously for 10 min. The aqueous phase was removed and MUAA (0.08 mmol) in DCM (2 mL) was added to the remaining yellowish organic phase. In a fast manner, sodium borohydride in water (37.8 mg, 2 mL) was added under intense stirring as the colour of the solution instantly changed to brownish red. When black precipitates started to form after several minutes, 2 mL of aqueous HCl (1 M) was added slowly and the mixture was stirred for another 10 min. Then, the colourless organic phase was removed, and the aqueous phase was transferred into a 50 mL falcon tube. Acetone (45 mL) was added, and the particles were centrifuged (8000 rpm, 5 min) and re-dispersed in water. After a second centrifugation step, the particles were re-dispersed in dry DMF (20 mL) and transferred to a reaction flask. Small amounts of triethylamine were added until the solution showed a slightly basic pH. (1R,8S,9s)-bicyclo[6.1.0]non-4-yn-9-ylmethyl N-succinimidyl carbonate (0.008 mmol) was added and the reaction was stirred overnight. The particles were purified by centrifugation in acetone and stored in DMF. For determination of the BCN-functionalization degree, 20 μL of Au-BCN in DMF (1 mg mL^{-1}) was mixed with 1 mL of dansyl azide in DMF (217 μM) for 24 h. The particles were centrifuged and the supernatant was measured by absorption spectroscopy. The amount of reacted azide was calculated by the difference of absorbance at 362 nm between the supernatant and a dansyl azide stock solution (217 μM). On the assumption of full conversion, the amount of BCN groups in the sample solution was set equal to the amount of reacted azides. The concentration of BCN groups in the Au-BCN stock solution was determined to be 2.4 μmol mL^{-1} or μmol mg^{-1} of particles, respectively.

4.5. Synthesis of AuNGs

N_3-tPG$_{6kDa}$-N_3 (1.7 μmol) and Au@BCN (1.4 μmol BCN units) were solubilized and mixed in DMF to obtain a total volume of 1 mL. The mixture was shortly stirred on a vortex stirrer and then instantly injected into water (20 mL) at 45 °C under vigorous stirring. After 16 h, 3-Azidopropanol in DMF (10 μL) was added to quench remaining alkyne groups. The AuNGs were dialysed against ultrapure water (MWCO = 50,000 Da) and concentrated by sedimentation.

4.6. Synthesis of GAuNGs

N_3-tPG$_{6kDa}$-N_3 (1.7 μmol) and Au@BCN (6 mg, 1.4 μmol BCN units) were solubilized and mixed in DMF to obtain a total volume of 1 mL. The mixture was shortly stirred on a vortex stirrer and then instantly injected into aqueous tetrachloroauric acid trihydrate solution (20 mL, 0.25 mM) with 20 μL of HCl (1 M) at 45 °C under vigorous stirring. Immediately afterwards, aqueous solutions of silver nitrate (200 μL, 3 mM) and ascorbic acid (50 μL, 100 mM) were added. After 16 h, 3-Azidopropanol in DMF (10 μL) was added to quench remaining alkyne groups. The GAuNGs were dialyzed against ultrapure water (MWCO = 50,000 Da) and concentrated by sedimentation. PEGylated GAuNGs for cell incubation studies were synthesized by adding mono-azidated PEG instead of 3-Azidopropanol for quenching of the reaction.

4.7. Photothermal conversion

The photothermal conversion of GAuNGs was determined by irradiation with a 785 nm laser (500 mW, 0.59 W cm^{-2}). Aliquots of 10 μL sample in aqueous solution at different concentrations were placed in an Eppendorf tube and continuously irradiated for 5 min from the top to the bottom of the tube. Changes in temperature were recorded in a 90° angle to the light beam by a FLIR E30 thermal imaging camera. The irradiation of all samples was started at room temperature (25 °C). The photothermal conversion efficiency η was calculated by measuring one heating and cooling cycle based on the literature according to Eq. (1) [57].

$$\eta = \frac{hA\Delta T_{max} - Q_s}{I\left(1 - 10^{A_{785nm}}\right)} \quad (1)$$

where h is the heat transfer coefficient, A is the surface area of the vessel, ΔT_{max} is the difference between starting temperature and maximum temperature, Q_S is the light absorbance of the solvent (determined to be 25.2 mW for water), I is the laser power, and A_{785nm} is the absorbance of GAuNGs at 785 nm. hA can be determined by calculating Eq. (2) for each timepoint of the cooling period and apply the linear time data versus -lnΘ according to Eq. (3), where m is the mass capacity and C_p the heat capacity of the solvent.

$$\Theta = \frac{T}{T_{max}} \quad (2)$$

$$t = \frac{\sum_i m_i C_{p,i}}{hA}\Theta \quad (3)$$

4.8. Drug loading and release of Dox

Hydrophobic Dox was synthesized by adding excess triethylamine to doxorubicin hydrochloride in water, followed by extraction with dichloromethane. Dox was loaded to the nanogels by mixing 200 μL of GAuNGs in water (5 mg mL^{-1}) with 1 mL of doxorubicin in THF (0.5, 1, 2, or 3 mg mL^{-1}) for 24 h at room temperature. The particles were centrifuged and the supernatant was measured by absorption spectroscopy at 570 nm to calculate the drug loading capacity (DLC (%) = (m of encapsulated drug × 100) / (m of GAuNG)) and encapsulation efficiency (EE (%) = (m of encapsulated drug × 100) / (m of initial drug)). DLC of 27.0% and EE of 13.5% were observed for 2 mg mL^{-1} Dox-solution. For drug release, GAuNG-Dox was washed 3 times by centrifugation and redispersion in water. After the last washing step, GAuNGs-Dox were redispersed in 1 mL of either PBS (pH 7.4) or acetic acid buffer (pH 5) and kept at 25 °C or 42 °C. At different time points, aliquots of the solution were taken, centrifuged, and measured by absorption spectroscopy at 570 nm to determine the amount of released Dox. For NIR triggered release, GAuNGs-Dox were irradiated with a 785 nm laser for 5 min at the beginning of the studied time frame and release was determined as described above.

4.9. Cell culture

HeLa cells were cultured in Roswell Park Memorial Institute 1640 (RPMI-1640, Fisher Scientific) cell culture medium supplemented with 10% fetal bovine serum (FBS), 1% penicillin/streptomycin and 1% non-essential amino acids. The cells were maintained at 37 °C and 5% CO_2.

4.10. MTT assay

100 μL of 1 × 10^5 cells mL^{-1} were seeded onto a 96-well plate and kept overnight at 37 °C and 5% CO_2. The medium was replaced for fresh medium with dilutions of the test compounds (in duplicates). After 48 h, the cells were incubated with 100 μL of 3-(4,5-dimethylthiazol-2-yl)-2,5-diphenyltetrazolium bromide (MTT, 5 mg mL^{-1}) per well. After incubation for 4 h at 37 °C and 5% CO_2, the supernatant was discarded and 100 μL isopropanol (0.04 M HCl) was added. Absorbance at 570 nm was read in a Tecan Infinite M200 Pro microplate reader. Assays were repeated three times independently. Relative cell viabilities were calculated by dividing the average absorbance values by the absorbance value of untreated cells.

4.11. Confocal scanning microscopy

1 mL of 1 × 10^5 cells mL^{-1} was seeded on 9 mm glass coverslips and kept overnight at 37 °C and 5% CO_2. The supernatant was replaced by fresh medium containing 100 μg mL^{-1} of particles. After incubation for 16 h, the cells were washed twice with 2 mL PBS and dispersed in fresh medium. Cell nuclei were stained with 4,6-diamidino-2-phenylindole (DAPI) and lysosomes with LysoTracker® Green DND-26 dye (Thermo Fisher). Images were captured with a CLSM Leica SP8 confocal laser scanning microscope.

4.12. In vitro photothermal therapy assay

2 mL of 5 × 10^4 cells mL^{-1} were seeded onto a 6-well plate and kept for 2 days at 37 °C and 5% CO2 until approximately 70% confluence were reached. The supernatant was replaced by fresh medium containing 100 μg mL^{-1}, 50 μg mL^{-1}, or 25 μg mL^{-1} of particles. After incubation for 24 h, the cells were washed twice with 2 mL PBS, trypsinized, transferred to 0.15 mL PCR tubes, and centrifuged for 4 min at 140 ×*g*. The supernatant was removed and the collected cells were irradiated with a 785 nm laser continuously for 3 min from above the tube with the lid open. The temperature was recorded with a FLIR infra-red camera. A second set of incubated cells was treated similarly except exposure to NIR-irradiation. Control cells were seeded and treated similarly with and without exposure to NIR-irradiation but incubated with medium only. After irradiation, the cells were re-suspended in 200 μL of fresh cell culture medium and 20 μL of the re-suspended cells were transferred to a 96-well-plate. After maintaining the cells at 37 °C and 5% CO_2 for 24 h, the relative cell viability was determined by MTT assay.

4.13. In vivo tolerability

The studies were performed in accordance with all national or local guidelines and regulations as described in the approved

Tierversuchsantrag G 0030/15 (Landesamt Berlin für Gesundheit) from 20.09.2018 for the EPO GmbH Berlin-Buch. For evaluating the tolerability of AuNGs and GAuNGs, female nude mice (NMRI, nu/nu) were treated with the nanogels. First, single doses of 10, 20, 40, 70 and 100 mg kg^{-1} were administered intravenously through the tail vein. The maximum tolerated dose of 100 mg kg^{-1} was then injected daily for five consecutive days. The body weight of the mice was monitored for 15 days. Afterwards, the mice were sacrificed and the organs (spleen, kidneys, liver, heart, lung) were collected for histopathology.

4.14. In vivo bioaccumulation

For bioaccumulation of the particles, female nude mice (NMRI, nu/nu) with adenocarcinoma were used. A549 adenocarcinomic human alveolar basal epithelial cells were cultured and transplanted subcutaneously into mice on day 0. A single dose of 100 mg kg^{-1} GAuNG was injected intravenously through the tail vein. Different groups of mice (n = 3 mice per group) were sacrificed after 2, 6, 12, 24, and 48 h. The organs (spleen, kidneys, liver, heart, lung, and tumor) were collected, homogenized in 500 μL of PBS, and dissolved in aqua regia (HCl/HNO_3 1:3) for 7 days. The samples were diluted and measured by ICP-OES determining the total amount of gold and silver.

4.15. In vivo therapy

For in vivo therapy, female nude mice (NMRI, nu/nu) with adenocarcinoma were used and split into different groups (n = 5 mice per group). A549 adenocarcinomic human alveolar basal epithelial cells were cultured and transplanted subcutaneously into mice on day 0. A single dose of 100 mg kg^{-1} GAuNG or GAuNG-Dox was injected intravenously through the tail vein on day 11 when the tumors reached a volume of approximately 0.1 cm^{-3}. Other groups were treated by subcutaneous injections of 30 μL (12 mg mL^{-1}) per 0.1 cm^{-3} tumor volume into the tumor. Irradiation with a 785 nm NIR laser (500 mW) was performed 24 h after intravenous or 5 min after intra-tumoral application from a distance of 5 cm to the tumor. After treatment, the mice were kept for further 21 days monitoring their tumor volume and body weight. Additional groups were treated similarly with injections of PBS or free Dox (8 mg kg^{-1}). After completion of the study the mice were sacrificed and tumors were dissected for weight measurement.

CRediT authorship contribution statement

Julian Bergueiro: Conceptualization; Data curation; Formal analysis; Investigation; Methodology; Supervision; Validation; Visualization; Writing - original draft; Writing - review & editing.

Emanuel A. Glitscher: Data curation; Formal analysis; Investigation; Methodology; Writing - original draft.

Marcelo Calderón: Conceptualization; Data curation; Formal analysis; Funding acquisition; Project administration; Resources; Supervision; Writing - review & editing.

Declaration of competing interest

The authors declare that they have no known competing financial interests or personal relationships that could have appeared to influence the work reported in this paper.

Acknowledgements

We gratefully acknowledge financial support from the Bundesministerium für Bildung und Forschung (BMBF) through the Nano-MatFutur award (13N12561, Thermonanogele). We would like to acknowledge the assistance of the Core Facility BioSupraMol supported by the Deutsche Forschungsgemeinschaft (DFG).

Appendix A. Supplementary data

Supplementary data to this article can be found online at https://doi.org/10.1016/j.bioadv.2022.212842.

References

[1] X. Yang, M. Yang, B. Pang, M. Vara, Y. Xia, Gold nanomaterials at work in biomedicine, Chem. Rev. 115 (2015) 10410–10488, https://doi.org/10.1021/acs.chemrev.5b00193.
[2] N. Khlebtsov, V. Bogatyrev, L. Dykman, B. Khlebtsov, S. Staroverov, A. Shirokov, L. Matora, V. Khanadeev, T. Pylaev, N. Tsyganova, G. Terentyuk, Analytical and theranostic applications of gold nanoparticles and multifunctional nanocomposites, Theranostics 3 (2013) 167–180, https://doi.org/10.7150/thno.5716.
[3] E.C. Dreaden, A.M. Alkilany, X. Huang, C.J. Murphy, M.A. El-Sayed, The golden age: gold nanoparticles for biomedicine, Chem. Soc. Rev. 41 (2011) 2740–2779, https://doi.org/10.1039/c1cs15237h.
[4] C.M. Cobley, J. Chen, E.C. Cho, L.V. Wang, Y. Xia, Gold nanostructures : a class of multifunctional materials for biomedical applications, Chem. Soc. Rev. 40 (2010) 44–56, https://doi.org/10.1039/b821763g.
[5] M. Pohanka, Current biomedical and diagnostic applications of gold micro and nanoparticles, Mini-Rev. Med. Chem. 21 (2021) 1085–1095, https://doi.org/10.2174/1389557520666200730155616.
[6] Y. Wu, M.R.K. Ali, K. Chen, N. Fang, M.A. El-Sayed, Gold nanoparticles in biological optical imaging, Nano Today 24 (2019) 120–140, https://doi.org/10.1016/j.nantod.2018.12.006.
[7] T. Repenko, A. Rix, A. Nedilko, J. Rose, A. Hermann, R. Vinokur, S. Moli, R. Cao-Milàn, M. Mayer, G. Plessen, A. Fery, L. Laporte, W. Lederle, D.N. Chigrin, A.J. C. Kuehne, Strong photoacoustic signal enhancement by coating gold nanoparticles with melanin for biomedical imaging, Adv. Funct. Mater. 28 (2018), 1705607, https://doi.org/10.1002/adfm.201705607.
[8] J. Song, J. Kim, S. Hwang, M. Jeon, S. Jeong, C. Kim, S. Kim, "Smart" gold nanoparticles for photoacoustic imaging: an imaging contrast agent responsive to the cancer microenvironment and signal amplification via pH-induced aggregation, Chem. Commun. 52 (2016) 8287–8290, https://doi.org/10.1039/c6cc03100e.
[9] J.P.M. Almeida, E.R. Figueroa, R.A. Drezek, Gold nanoparticle mediated cancer immunotherapy, Nanomedicine 10 (2014) 503–514, https://doi.org/10.1016/j.nano.2013.09.011.
[10] X.-M. Zhu, C. Fang, H. Jia, Y. Huang, C.H.K. Cheng, C.-H. Ko, Z. Chen, J. Wang, Y.-X.J. Wang, Cellular uptake behaviour, photothermal therapy performance, and cytotoxicity of gold nanorods with various coatings, Nanoscale 6 (2014) 11462–11472, https://doi.org/10.1039/c4nr03865g.
[11] N.S. Abadeer, C.J. Murphy, Recent Progress in cancer thermal therapy using gold nanoparticles, J. Phys. Chem. C 120 (2016) 4691–4716, https://doi.org/10.1021/acs.jpcc.5b11232.
[12] S.S. Lucky, K.C. Soo, Y. Zhang, Nanoparticles in photodynamic therapy, Chem. Rev. 115 (2015) 1990–2042, https://doi.org/10.1021/cr5004198.
[13] Z. Zhou, J. Zhao, Z. Di, B. Liu, Z. Li, X. Wu, L. Li, Core–shell gold nanorod@mesoporous-MOF heterostructures for combinational phototherapy, Nanoscale 13 (2020) 131–137, https://doi.org/10.1039/d0nr07681c.
[14] Y. Liu, P. Bhattarai, Z. Dai, X. Chen, Photothermal therapy and photoacoustic imaging via nanotheranostics in fighting cancer, Chem. Soc. Rev. 48 (2019) 2053–2108, https://doi.org/10.1039/c8cs00618k.
[15] X. Wang, G. Li, Y. Ding, S. Sun, Understanding the photothermal effect of gold nanostars and nanorods for biomedical applications, RSC Adv. 4 (2014) 30375–30383, https://doi.org/10.1039/c4ra02978j.
[16] N.N.M. Adnan, Y.Y. Cheng, N.M.N. Ong, T.T. Kamaruddin, E. Rozlan, T. W. Schmidt, H.T.T. Duong, C. Boyer, Effect of gold nanoparticle shapes for phototherapy and drug delivery, Polym. Chem. UK 7 (2016) 2888–2903, https://doi.org/10.1039/c6py00465b.
[17] P.K. Jain, K.S. Lee, I.H. El-Sayed, M.A. El-Sayed, Calculated absorption and scattering properties of gold nanoparticles of different size, shape, and composition: applications in biological imaging and biomedicine, J. Phys. Chem. B 110 (2006) 7238–7248, https://doi.org/10.1021/jp057170o.
[18] N. Li, P. Zhao, D. Astruc, Anisotropic gold nanoparticles: synthesis, properties, applications, and toxicity, Angew. Chem. Int. Ed. 53 (2014) 1756 1789, https://doi.org/10.1002/anie.201300441.
[19] M. Grzelczak, J. Pérez-Juste, P. Mulvaney, L.M. Liz-Marzán, Shape control in gold nanoparticle synthesis, Chem. Soc. Rev. 37 (2008) 1783–1791, https://doi.org/10.1039/b711490g.
[20] X. Lu, M. Rycenga, S.E. Skrabalak, B. Wiley, Y. Xia, Chemical synthesis of novel plasmonic nanoparticles, Annu. Rev. Phys. Chem. 60 (2009) 167–192, https://doi.org/10.1146/annurev.physchem.040808.090434.
[21] S.C. Nguyen, Q. Zhang, K. Manthiram, X. Ye, J.P. Lomont, C.B. Harris, H. Weller, A. P. Alivisatos, Study of heat transfer dynamics from gold nanorods to the environment via time-resolved infrared spectroscopy, ACS Nano 10 (2016) 2144–2151, https://doi.org/10.1021/acsnano.5b06623.
[22] M.L. Brongersma, N.J. Halas, P. Nordlander, Plasmon-induced hot carrier science and technology, Nat. Nanotechnol. 10 (2015) 25–34, https://doi.org/10.1038/nnano.2014.311.
[23] M. Kar, L. Fechner, G. Nagel, E. Glitscher, G.N. Rimondino, M. Calderón, Nanogels for biomedical applications, Smart Mater. Ser. (2018) 210–260, https://doi.org/10.1039/9781788010481-00210.

[24] Z. Zhang, J. Wang, X. Nie, T. Wen, Y. Ji, X. Wu, Y. Zhao, C. Chen, Near infrared laser-induced targeted cancer therapy using thermoresponsive polymer encapsulated gold nanorods, J. Am. Chem. Soc. 136 (2014) 7317–7326, https://doi.org/10.1021/ja412735p.
[25] Y. Zhong, C. Wang, R. Cheng, L. Cheng, F. Meng, Z. Liu, Z. Zhong, cRGD-directed, NIR-responsive and robust AuNR/PEG–PCL hybrid nanoparticles for targeted chemotherapy of glioblastoma in vivo, J. Control. Release 195 (2014) 63–71, https://doi.org/10.1016/j.jconrel.2014.07.054.
[26] J. Yang, D. Shen, L. Zhou, X. Li, C. Yao, R. Wang, A.M. El-Toni, F. Zhang, D. Zhao, Spatially confined fabrication of core-shell gold nanocages@Mesoporous silica for near-infrared controlled photothermal drug release, Chem. Mater. 25 (2013) 3030 3037, https://doi.org/10.1021/cm401115b.
[27] D. Peer, J.M. Karp, S. Hong, O.C. Farokhzad, R. Margalit, R. Langer, Nanocarriers as an emerging platform for cancer therapy, Nat. Nanotechnol. 2 (2007) 751–760, https://doi.org/10.1038/nnano.2007.387.
[28] A.R. Guerrero, N. Hassan, C.A. Escobar, F. Albericio, M.J. Kogan, E. Araya, Gold nanoparticles for photothermally controlled drug release, Nanomedicine-Uk 9 (2014) 2023–2039, https://doi.org/10.2217/nnm.14.126.
[29] E.C. Dreaden, L.A. Austin, M.A. Mackey, M.A. El-Sayed, Size matters: gold nanoparticles in targeted cancer drug delivery, Ther. Deliv. 3 (2012) 457–478, https://doi.org/10.4155/tde.12.21.
[30] M. Molina, M. Asadian-Birjand, J. Balach, J. Bergueiro, E. Miceli, M. Calderón, Stimuli-responsive nanogel composites and their application in nanomedicine, Chem. Soc. Rev. 44 (2015) 6161–6186, https://doi.org/10.1039/c5cs00199d.
[31] X. Zhang, S. Malhotra, M. Molina, R. Haag, Micro- and nanogels with labile crosslinks – from synthesis to biomedical applications, Chem. Soc. Rev. 44 (2015) 1948–1973, https://doi.org/10.1039/c4cs00341a.
[32] H.-Q. Wu, C.-C. Wang, Biodegradable smart nanogels: a new platform for targeting drug delivery and biomedical diagnostics, Langmuir 32 (2016) 6211–6225, https://doi.org/10.1021/acs.langmuir.6b00842.
[33] A.E. Ekkelenkamp, M.R. Elzes, J.F.J. Engbersen, J.M.J. Paulusse, Responsive crosslinked polymer nanogels for imaging and therapeutics delivery, J. Mater. Chem. B 6 (2017) 210–235, https://doi.org/10.1039/c7tb02239e.
[34] J. Bergueiro, M. Calderón, Thermoresponsive nanodevices in biomedical applications, Macromol. Biosci. 15 (2015) 183–199, https://doi.org/10.1002/mabi.201400362.
[35] Y. Yin, B. Hu, X. Yuan, L. Cai, H. Gao, Q. Yang, Nanogel: a versatile nano-delivery system for biomedical applications, Pharmacy 12 (2020) 290, https://doi.org/10.3390/pharmaceutics12030290.
[36] D.E. Thrall, P. Maccarini, P. Stauffer, J. Macfall, M. Hauck, S. Snyder, B. Case, K. Linder, L. Lan, L. Mccall, M.W. Dewhirst, Thermal dose fractionation affects tumour physiological response, Int. J. Hyperth. 28 (2012) 431–440, https://doi.org/10.3109/02656736.2012.689087.
[37] Y. Yang, J. Aw, B. Xing, Nanostructures for NIR light-controlled therapies, Nanoscale 9 (2017) 3698–3718, https://doi.org/10.1039/c6nr09177f.
[38] H.S. El-Sawy, A.M. Al-Abd, T.A. Ahmed, K.M. El-Say, V.P. Torchilin, Stimuli-responsive nano-architecture drug-delivery systems to solid tumor micromilieu: past, present, and future perspectives, ACS Nano 12 (2018) 10636–10664, https://doi.org/10.1021/acsnano.8b06104.
[39] X. Lian, J. Jin, J. Tian, H. Zhao, Thermoresponsive nanohydrogels cross-linked by gold nanoparticles, ACS Appl. Mater. Interfaces 2 (2010) 2261–2268, https://doi.org/10.1021/am1003156.
[40] O.S. Muddineti, B. Ghosh, S. Biswas, Current trends in using polymer coated gold nanoparticles for cancer therapy, Int. J. Pharm. 484 (2015) 252–267, https://doi.org/10.1016/j.ijpharm.2015.02.038.
[41] A. Thomas, S.S. Müller, H. Frey, Beyond Poly(ethylene glycol): linear polyglycerol as a multifunctional polyether for biomedical and pharmaceutical applications, Biomacromolecules 15 (2014) 1935–1954, https://doi.org/10.1021/bm5002608.
[42] S. Aoki, A. Koide, S. Imabayashi, M. Watanabe, Novel thermosensitive polyethers prepared by anionic ring-opening polymerization of glycidyl ether derivatives, Chem. Lett. 31 (2002) 1128–1129, https://doi.org/10.1246/cl.2002.1128.
[43] B. Schulte, A. Walther, H. Keul, M. Möller, Polyglycidol-based prepolymers to tune the nanostructure of microgels, Macromolecules 47 (2014) 1633–1645, https://doi.org/10.1021/ma401465c.
[44] M. Asadian-Birjand, J. Bergueiro, F. Rancan, J.C. Cuggino, R.-C. Mutihac, K. Achazi, J. Dernedde, U. Blume-Peytayi, A. Vogt, M. Calderón, Engineering thermoresponsive polyether-based nanogels for temperature dependent skin penetration, Polym. Chem. 6 (2015) 5827–5831, https://doi.org/10.1039/c5py00924c.
[45] L. Zhou, J. Geng, G. Wang, J. Liu, B. Liu, Facile synthesis of stable and water-dispersible multihydroxy conjugated polymer nanoparticles with tunable size by dendritic cross-linking, ACS Macro Lett. 1 (2012) 927–932, https://doi.org/10.1021/mz300282s.
[46] E. Cazares-Cortes, A. Espinosa, J.-M. Guigner, A. Michel, N. Griffete, C. Wilhelm, C. Ménager, Doxorubicin intracellular remote release from biocompatible Oligo (ethylene glycol) methyl ether methacrylate-based magnetic nanogels triggered by magnetic hyperthermia, ACS Appl. Mater. Interfaces 9 (2017) 25775–25788, https://doi.org/10.1021/acsami.7b06553.
[47] J.-Y. Kim, W.I. Choi, M. Kim, G. Tae, Tumor-targeting nanogel that can function independently for both photodynamic and photothermal therapy and its synergy from the procedure of PDT followed by PTT, J. Control. Release 171 (2013) 113–121, https://doi.org/10.1016/j.jconrel.2013.07.006.
[48] E. Lallana, R. Riguera, E. Fernandez-Megia, Reliable and efficient procedures for the conjugation of biomolecules through huisgen azide-alkyne cycloadditions, Angew. Chem. Int. Ed. 50 (2011) 8794–8804, https://doi.org/10.1002/anie.201101019.
[49] J.C. Jewett, C.R. Bertozzi, Cu-free click cycloaddition reactions in chemical biology, Chem. Soc. Rev. 39 (2010) 1272–1279, https://doi.org/10.1039/b901970g.
[50] J.C. Cuggino, C.I.A. I, M.C. Strumia, P. Welker, K. Licha, D. Steinhilber, R.-C. Mutihac, M. Calderón, Thermosensitive nanogels based on dendritic polyglycerol and N-isopropylacrylamide for biomedical applications, Soft Matter 7 (2011) 11259–11266, https://doi.org/10.1039/c1sm06357j.
[51] M. Giulbudagian, M. Asadian-Birjand, D. Steinhilber, K. Achazi, M. Molina, M. Calderón, Fabrication of thermoresponsive nanogels by thermo-nanoprecipitation and in situ encapsulation of bioactives, Polym. Chem. 5 (2014) 6909–6913, https://doi.org/10.1039/c4py01186d.
[52] H. Kobayashi, B. Turkbey, R. Watanabe, P.L. Choyke, Cancer drug delivery: considerations in the rational design of nanosized bioconjugates, Bioconjug. Chem. 25 (2014) 2093 2100, https://doi.org/10.1021/bc500481x.
[53] M. Brust, M. Walker, D. Bethell, D.J. Schiffrin, R. Whyman, Synthesis of thiol-derivatised gold nanoparticles in a two-phase liquid-liquid system, J. Chem. Soc. Chem. Commun. (1994) 801–802, https://doi.org/10.1039/c39940000801.
[54] M. Asadian-Birjand, C. Biglione, J. Bergueiro, A. Cappelletti, C. Rahane, G. Chate, J. Khandare, B. Klemke, M.C. Strumia, M. Calderón, Transferrin decorated thermoresponsive nanogels as magnetic trap devices for circulating tumor cells, Macromol. Rapid Commun. 37 (2015) 439–445, https://doi.org/10.1002/marc.201500590.
[55] H. Yuan, C.G. Khoury, H. Hwang, C.M. Wilson, G.A. Grant, T. Vo-Dinh, Gold nanostars: surfactant-free synthesis, 3D modelling, and two-photon photoluminescence imaging, Nanotechnology 23 (2012), 075102, https://doi.org/10.1088/0957-4484/23/7/075102.
[56] J. Gao, X. Huang, H. Liu, F. Zan, J. Ren, Colloidal stability of gold nanoparticles modified with thiol compounds: bioconjugation and application in cancer cell imaging, Langmuir 28 (2012) 4464–4471, https://doi.org/10.1021/la204289k.
[57] Y. Liu, K. Ai, J. Liu, M. Deng, Y. He, L. Lu, Dopamine-melanin colloidal nanospheres: an efficient near-infrared photothermal therapeutic agent for in vivo cancer therapy, Adv. Mater. 25 (2013) 1353–1359, https://doi.org/10.1002/adma.201204683.
[58] W. Mao, H.S. Kim, Y.J. Son, S.R. Kim, H.S. Yoo, Doxorubicin encapsulated clicked gold nanoparticle clusters exhibiting tumor-specific disassembly for enhanced tumor localization and computerized tomographic imaging, J. Control. Release 269 (2018) 52–62, https://doi.org/10.1016/j.jconrel.2017.11.003.
[59] Z. Zhang, Y. Wang, S. Xu, Y. Yu, A. Hussain, Y. Shen, S. Guo, Photothermal gold nanocages filled with temperature sensitive tetradecanol and encapsulated with glutathione responsive polycurcumin for controlled DOX delivery to maximize anti-MDR tumor effects, J. Mater. Chem. B 5 (2017) 5464–5472, https://doi.org/10.1039/c7tb01253e.
[60] X. Cheng, X. Tian, A. Wu, J. Li, J. Tian, Y. Chong, Z. Chai, Y. Zhao, C. Chen, C. Ge, Protein Corona influences cellular uptake of gold nanoparticles by phagocytic and nonphagocytic cells in a size-dependent manner, ACS Appl. Mater. Interfaces 7 (2015) 20568–20575, https://doi.org/10.1021/acsami.5b04290.
[61] R. García-Álvarez, M. Hadjidemetriou, A. Sánchez-Iglesias, L.M. Liz-Marzán, K. Kostarelos, In vivo formation of protein corona on gold nanoparticles. The effect of their size and shape, Nanoscale 10 (2017) 1256–1264, https://doi.org/10.1039/c7nr08322j.
[62] N. Feliu, X. Sun, R.A.A. Puebla, W.J. Parak, Quantitative particle-cell interaction: some basic physicochemical pitfalls, Langmuir 33 (2017) 6639–6646, https://doi.org/10.1021/acs.langmuir.6b04629.
[63] X. Ma, R. Hartmann, D.J. de Aberasturi, F. Yang, S.J.H. Soenen, B.B. Manshian, J. Franz, D. Valdeperez, B. Pelaz, N. Feliu, N. Hampp, C. Riethmüller, H. Vieker, N. Frese, A. Gölzhäuser, M. Simonich, R.L. Tanguay, X.-J. Liang, W.J. Parak, Colloidal gold nanoparticles induce changes in cellular and subcellular morphology, ACS Nano 11 (2017) 7807–7820, https://doi.org/10.1021/acsnano.7b01760.
[64] N. Khlebtsov, L. Dykman, Biodistribution and toxicity of engineered gold nanoparticles : a review of in vitro and in vivo studies, Chem. Soc. Rev. 40 (2010) 1647–1671, https://doi.org/10.1039/c0cs00018c.
[65] A.M. Alkilany, P.K. Nagaria, C.R. Hexel, T.J. Shaw, C.J. Murphy, M.D. Wyatt, Cellular uptake and cytotoxicity of gold nanorods: molecular origin of cytotoxicity and surface effects, Small 5 (2009) 701–708, https://doi.org/10.1002/smll.200801546.
[66] S.J. Soenen, B.B. Manshian, A.M. Abdelmonem, J. Montenegro, S. Tan, L. Balcaen, F. Vanhaecke, A.R. Brisson, W.J. Parak, S.C.D. Smedt, K. Braeckmans, The cellular interactions of PEGylated gold nanoparticles: effect of PEGylation on cellular uptake and cytotoxicity, Part. Part. Syst. Charact. 31 (2014) 794–800, https://doi.org/10.1002/ppsc.201300357.
[67] D.A. Giljohann, D.S. Seferos, W.L. Daniel, M.D. Massich, P.C. Patel, C.A. Mirkin, Gold nanoparticles for biology and medicine, Angew. Chem. Int. Ed. 49 (2010) 3280–3294, https://doi.org/10.1002/anie.200904359.
[68] S. Mercier, D. Breuillé, L. Mosoni, C. Obled, P.P. Mirand, Chronic inflammation alters protein metabolism in several organs of adult rats, J. Nutr. 132 (2002) 1921–1928, https://doi.org/10.1093/jn/132.7.1921.
[69] E.A. Repasky, S.S. Evans, M.W. Dewhirst, Temperature matters! And why it should matter to tumor immunologists, Cancer Immunol. 1 (2013) 210–216, https://doi.org/10.1158/2326-6066.cir-13-0118.
[70] C. Wang, H. Xu, C. Liang, Y. Liu, Z. Li, G. Yang, L. Cheng, Y. Li, Z. Liu, Iron oxide @ polypyrrole nanoparticles as a multifunctional drug carrier for remotely controlled

cancer therapy with synergistic antitumor effect, ACS Nano 7 (2013) 6782–6795, https://doi.org/10.1021/nn4017179.

[71] K. Harmrolfs, L. Mancuso, B. Drung, F. Sasse, A. Kirschning, Preparation of new alkyne-modified ansamitocins by mutasynthesis, Beilstein J. Org. Chem. 10 (2014) 535–543, https://doi.org/10.3762/bjoc.10.49.

[72] M. Gervais, A.-L. Brocas, G. Cendejas, A. Deffieux, S. Carlotti, Synthesis of linear high molar mass glycidol-based polymers by monomer-activated anionic polymerization, Macromolecules 43 (2010) 1778–1784, https://doi.org/10.1021/ma902286a.